



ELSEVIER

Contents lists available at ScienceDirect

Journal of Luminescence

journal homepage: www.elsevier.com/locate/jlumin

A modified energy transfer model for determination of upconversion emission of β -NaYF₄:Yb,Er: Role of self-quenching effect

Hongyuan Zhu^{a,b}, Min Lin^{a,b,*}, Guorui Jin^{a,b}, Tian Jian Lu^b, Feng Xu^{a,b}^a The Key Laboratory of Biomedical Information Engineering, Ministry of Education, School of Life Science and Technology, Xi'an Jiaotong University, Xi'an 710049, PR China^b Bioinspired Engineering and Biomechanics Center (BEBC), Xi'an Jiaotong University, Xi'an 710049, PR China

ARTICLE INFO

Article history:

Received 8 July 2016

Received in revised form

11 January 2017

Accepted 13 January 2017

Available online 20 January 2017

Keywords:

Upconversion emission

Energy transfer

Concentration quenching

Self-quenching effect

ABSTRACT

A modified energy transfer model by incorporating self-quenching effect is introduced to determine upconversion emission of β -NaYF₄:Yb,Er. The simulation results agree well with existing experimental results, demonstrating the critical role of self-quenching effect in upconversion emission. Our results confirm that a 4.4-fold increase of green upconversion and 86-fold increase in the intensity of red upconversion emission could be realized by suppressing self-quenching. In addition, the optimal doping concentrations for integral emission intensity are found to be independent of excitation power, while the green to red ratio is found to rely significantly on excitation power. Our model offers mechanistic insight into upconversion emission processes and provides inspirations in improving upconversion emission efficiency through optimization of energy transfer pathways in different types of matrix sub-lattice.

© 2017 Elsevier B.V. All rights reserved.

1. Introduction

The rare earth up-conversion (UC) phosphors that convert near-infrared emission into ultra-violet or visible emission have shown widespread applications in various fields [1]. The UC emission has been found to be affected by doping concentration in various host materials such as oxide, sulfide, fluoride and heavy halide [2]. For example, the most common doping concentration for Yb³⁺/Er³⁺ doped UC phosphors are 1–2% Er³⁺ and 10–20% Yb³⁺ [3–8]. Further increasing of doping concentration will decrease the emission intensity of these UC phosphors due to the concentration quenching effect found in various experiments [4,5]. Although a number of energy back transfer and cross relaxation pathways have been proposed to understand concentration quenching, the underlying mechanisms remain elusive [7–10].

Besides back energy transfer and cross relaxation, self-quenching also contributes to the concentration quenching [11]. Self-quenching is a process that energy diffusion to nonradiative energy sink among the same dopant ions [11–13]. Self-quenching involves three sub-processes, including the energy diffusion among the same state of donors, energy transfer towards nonradiative sinks and the energy dissipation (nonradiative decay) caused by extrinsic sinks (constituted by a nonradiative species or “poisonous center”). Self-

quenching effect has been found to occur at the first excited states of various ions in a number of host matrix, such as Yb³⁺ doped Y₂O₃, Gd₂O₃ [11], borate glasses [14], NaYF₄ [15], and Er³⁺ doped Y₂O₃ [12], NaYF₄ [16]. Therefore, self-quenching effect of Er³⁺ and Yb³⁺ could also play an important role in UC emission of Yb³⁺/Er³⁺ ion pair doped UC phosphors with increasing Er³⁺ and Yb³⁺ concentrations, which has not been explored yet.

In the previous works, mathematical models based on rate-equations have been used to understand excitation power dependent upconversion emission [17], energy transfer pathways underlying upconversion processes [18], time evolution of upconversion emission [15], plasmon enhanced upconversion emission [19], and quantitatively determination of rate constants values for energy transfer by fitting the simulated life-time with experimental results [20]. These studies have incorporated energy back transfer and cross relaxation processes. However, self-quenching is another possible pathway related to doping concentration dependent change in upconversion emission behavior, which haven't been explored yet.

In this contribution, we proposed a modified energy transfer model by incorporating self-quenching effect to provide the mechanistic insight into the concentration quenching phenomenon observed in former experiments. The simulation results are consistent with the existing experimental results. The simulated relative integral emission intensity and green to red ratio fall in the reasonable range among the experimental results. The proposed model thus provides us with deep understanding of the UC emission of Yb³⁺/Er³⁺ ion doped UC phosphor and paves the way for designing UC nanoparticles with the optimized emission efficiency.

* Corresponding author at: The Key Laboratory of Biomedical Information Engineering, Ministry of Education, School of Life Science and Technology, Xi'an Jiaotong University, Xi'an 710049, PR China.

E-mail address: minlin@mail.xjtu.edu.cn (M. Lin).

2. Theoretical methods

In the UC emission process, ground state absorption, excited state absorption and energy transfer upconversion (ETU) are responsible for higher energy photon emission. Besides the absorption and ETU processes, the radiative decay, nonradiative multiphonon relaxation (MPR), cross relaxation (CR) and energy back transfer (EBT) coexist during UC emission process. The kinetics of UC emission process could be described by a set of rate equations [17,18]:

$$\begin{aligned} dN_i/dt = & \sum_j (A_{ji}N_j - A_{ij}N_i) + (W_{mi}^A N_m - W_{ij}^A N_i) \\ & + (W_{i+1,i}^{NR} N_{i+1} - W_{i,i-1}^{NR} N_i) + \sum_{ij,kl} (P_{ji,ik}^{ET} N_j N_l - P_{ij,kl}^{ET} N_i N_k) \end{aligned} \quad (1)$$

where i, j, k, l and m represent different ground or excited states; N_i (nm^{-3}) is the population of state i ; A_{ij} (s^{-1}) is the Einstein coefficients for radiative transitions from state i to j ; W_{ij}^{NR} (s^{-1}) is the nonradiative multiphonon relaxation rate from the state i to the state immediately below i ; $P_{ij,kl}^{ET}$ ($\text{nm}^3 \text{s}^{-1}$) is the microscopic energy transfer parameter for the transfer of energy for the donor i to j transition and the acceptor k to l transition. W_{mi}^A (s^{-1}) is the absorption rate of state m . The calculation processes and values of all these parameters could be found in Appendix A, Tables A1–A5.

To explain concentration quenching, Er–Yb interactions have been considered in energy transfer terms as shown in the standard energy transfer model (Eq. 1). While self-quenching effect is a separate mechanism which is independent of Er–Yb interactions (including energy back transfer) that contributes to UC emission. Whereas both Er–Yb interactions and self-quenching effect contribute to concentration dependent UC emission. To consider the self-quenching effect caused by energy migration among the dopant ions, we added a self-quenching effect term to Eq. (1):

$$\begin{aligned} dN_i/dt = & \sum_j (A_{ji}N_j - A_{ij}N_i) + (W_{mi}^A N_m - W_{ij}^A N_i)(W_{i+1,i}^{NR} N_{i+1} \\ & - W_{i,i-1}^{NR} N_i) + \sum_{ij,kl} (P_{ji,ik}^{ET} N_j N_l - P_{ij,kl}^{ET} N_i N_k) - R_i^Q N_i \end{aligned} \quad (2)$$

where R_i^Q (s^{-1}) is the self-quenching rate constant of state i , and $R_i^Q N_i$ ($\text{nm}^{-3} \text{s}^{-1}$) represents depopulation rate of state i by self-quenching effect. A set of rate equations (Eqs. A1–A10) of $\text{Yb}^{3+}/\text{Er}^{3+}$ doped phosphors expanded from Eq. (2) could be found in Appendix A.

In limited diffusion case, self-quenching in UC phosphors is ruled by the non-radiative energy transfer process rather than nonradiative quenching transition to defects [12]. Thus the self-quenching probability can be considered comparable to the transfer probability for diffusion [12]. Considering that electric dipole-dipole interaction is usually the main process of energy transfer, the self-quenching behavior can be depicted by the function of lifetime τ_i with doping concentration N_{RE} as [12]:

$$\tau_i(N_{RE}) = \tau_{wi} [1 + (9/2\pi)(N_{RE}/N_{0,i})^2] \quad (3)$$

where τ_{wi} is lifetime of state i at infinite low doping concentration, $N_{0,i}$ (nm^{-3}) is the critical concentration where non-radiative energy transfer probability approximates to that of photon emission [12]. Then we can obtain self-quenching rate constant R_i^Q as:

$$R_i^Q = \frac{1}{\tau(N_{RE})} - \frac{1}{\tau_{wi}} = \frac{9}{2\pi} \frac{1}{\tau_{wi}} \left(\frac{N_{RE}}{N_{0,i}} \right)^2 \quad (4)$$

Obviously self-quenching rate constant is square of doping concentration in limited diffusion case, the self-quenching rate

constant can be given by [11]:

$$R_i^Q = K_i N_{RE}^2 \quad (5)$$

where K_i ($\text{nm}^6 \text{s}^{-1}$) is a constant independent of doping concentration.

Self-quenching occurs because of the energy migration among doping sites and finally quenched by defects inside the matrix or ligands on the surface [11]. Self-quenching may occur on any excited states with varying self-quenching rate constants. For $\text{NaYF}_4:\text{Yb,Er}$, the main UC emission states are green and red emission states. Therefore, we considered self-quenching on ${}^4\text{F}_{9/2}$ (red emission state), ${}^4\text{S}_{3/2}$ (green emission state) of Er^{3+} and ${}^2\text{F}_{5/2}$ of Yb^{3+} in the modified model. The calculation processes and results of self-quenching rate constants are shown in Appendix A.

We therefore simplified the model by considering self-quenching only on ${}^4\text{S}_{3/2}$ of Er^{3+} and ${}^2\text{F}_{5/2}$ of Yb^{3+} , and the rate constant of self-quenching effect could be represented by K_{Er6} and K_{Yb} respectively (See Appendix A, Table A1).

The emission intensity I_i ($\text{nm}^{-3} \text{s}^{-1}$) of state i in our model could be defined as

$$I_i = A_{if} N_i \quad (6)$$

where A_{if} (s^{-1}) is the radiative decay rate from state i to the ground state.

Self-quenching is a process that energy on excited ions migrates to internal or surface defects. Surface quenching is only a part of self-quenching which could be negligible in large particles. While energy migrates to internal defects contributes mainly to the self-quenching in large sized powders [12]. Thus, size effect on UC emission intensity is not considered in this work for we set our model for large NaYF_4 particles.

The proposed major UC emission process in $\text{Yb}^{3+}/\text{Er}^{3+}$ doped $\beta\text{-NaYF}_4$ under low power excitation ($< 100 \text{ W/cm}^2$) (Fig. 1) was summarized from references [7–10,17]. The rate equation Eq. (2) was solved by Euler method [20]. Simulation time period is 50 ms to reach a steady state by the end of the simulation time period. The calculation time step is 10 ns.

To analyze the main pathways associated with the green and red emission processes, we considered only transitions with highest branching fractions β_{ij} and contribution fractions κ_{ji} as the same method adopted in reference [18], where

$$\beta_{ij} = \frac{(dN_i/dt)_{i \rightarrow j}^t}{\sum_{t=A, RD, MPR, ET, SQ} \sum_m (dN/dt)_{i \rightarrow m}^t} \quad (7)$$

$$\kappa_{ji} = \frac{(dN_i/dt)_{j \rightarrow i}^t}{\sum_t \sum_m (dN/dt)_{m \rightarrow i}^t} \quad (8)$$

For a given transition type t (absorption, radiation decay, multiphonon relaxation, energy transfer, self-quenching) from i to j , the rates $(dN_i/dt)_{i \rightarrow j}^t$ in Eq. (7) represent rates of branch transitions (processes consuming the population) on state i , and could be obtained by corresponding negative components in Eq. (2). Similarly, the rates $(dN_i/dt)_{j \rightarrow i}^t$ in Eq. (8) represent rates of contribution transitions (processes feeding the population) on state j , and could be obtained by corresponding positive components in Eq. (2). $\sum_t \sum_m (dN/dt)_{i \rightarrow m}^t$ represents total rate of branch transitions on state i and $\sum_t \sum_m (dN/dt)_{m \rightarrow i}^t$ represents total rate of contribution transitions on state i . $\beta_{ij}(\kappa_{ji})$ represents transition's fractional contribution to the overall depletion (population) of i by all types of transitions to (from) level j . When the UC phosphor is continuously excited, the

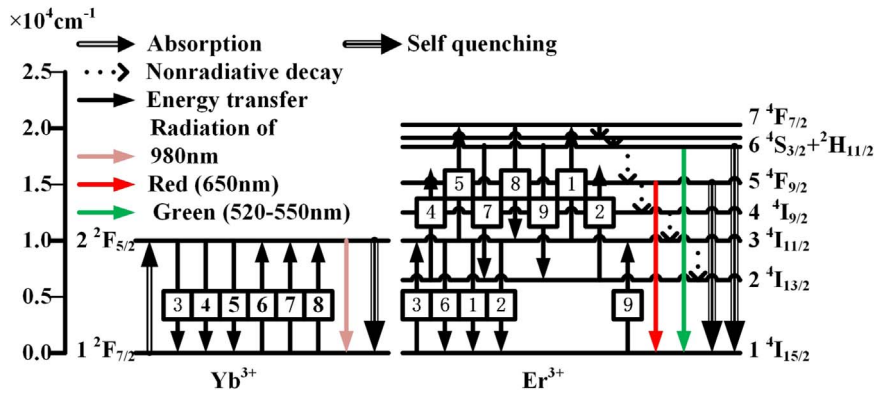


Fig. 1. Scheme of major UC emission processes in $\text{Yb}^{3+}/\text{Er}^{3+}$ doped $\beta\text{-NaYF}_4$ under low power excitation. The serial numbers of energy transfer processes represent as 1–5: ETU 0–4, 6–8: EBT 2–4, 9: CR respectively.

population of each state reaches an equilibrium. Under this equilibrium condition, the summation time derivatives are zero, namely, $\frac{dN_i}{dt} = -\sum_t \sum_m (dN/dt)_{i \rightarrow m}^t + \sum_t \sum_m (dN/dt)_{m \rightarrow i}^t = 0$. This relationship could be used to determine the simulation time period.

3. Results and discussion

3.1. Pathway analysis of green and red emission

To check if our modified model could simulate the widely accepted main energy pathways in UC emission, we compared the simulation results from our modified model with the existing model (i.e., Eq. 1). As listed in Tables B1 and B2 (Appendix B), β_{ij} and κ_{ij} of main energy pathways of each state show no significant difference between our modified model and the standard model. The simulated results indicate that our modified model could capture the widely accepted main energy pathways except the self-quenching processes we incorporated.

The results shown in Appendix B, Tables B1 and B2 indicate that green emission (summation of population of $4^4\text{S}_{3/2}$ and $2^2\text{H}_{11/2}$) is mainly related to $4^4\text{F}_{7/2}$, $4^4\text{S}_{3/2}$, $2^2\text{H}_{11/2}$, $4^4\text{I}_{11/2}$ states of Er^{3+} and $2^2\text{F}_{5/2}$ of Yb^{3+} . Also, ETU 2, 4, EBT 2, 4, CR, absorption of Yb^{3+} , and radiative/nonradiative decay from corresponding states, self-quenching processes of Er^{3+} and Yb^{3+} are the main process to be considered.

Berry has shown that red emission could be attributed mainly to energy back transfer from $\text{Er}^{3+}(^4\text{G}^2\text{K})$ to $\text{Yb}^{3+}(^2\text{F}_{7/2})$ [21]. However different experimental conditions (e.g., different pump power) may lead to a different upconversion emission mechanism [22]. As contrary to Berry's conclusion that three photon pathway could be a major process feeding red emission, two photon pathways are found to dominate red emission under low power continuous excitation [23,24]. Jung et al., found that red emission intensity is proportional to 1.99th power of excitation power at low excitation power region ($< 50 \text{ W} \cdot \text{cm}^{-2}$), which indicates that three photon process is not important under this condition [23]. However, the red emission could increase faster than green emission (the intensity is 1.76th power of excitation power) [23]. This suggests that there is a two photon ETU process that contributes to red emission separate from MPR of $4^4\text{S}_{3/2}$. This is why ETU3 is considered as a major contribution process to red emission state in this study. In our study, we established our model at the same excitation condition with Jung's [23]. We found that in NaYF_4 : 20%Yb, 2%Er, even though with a low rate constant ($7.05 \cdot 10^2 \text{ nm}^3 \text{ s}^{-1}$), ETU3 could also be a primary contribution transition to $4^4\text{F}_{9/2}$ (contribution fraction is larger than 55%, see in Table B1). We therefore excluded the transitions related to states

higher than $4^4\text{F}_{7/2}(\text{Er}^{3+})$ and attributed the red upconversion emission mechanism mainly to ETU3 and nonradiative decay from green emission states.

3.2. Model verification

To verify our model, we compared simulation results (from our modified model and the standard model) with the reported experimental results (Fig. 2) [4,5]. The relative integral intensity (normalized to integral intensity with doping of 10% Yb, 2% Er) and green to red ratio as a function of Yb^{3+} concentration (ranging from 10–50%) at fixed 2% Er^{3+} are shown in Fig. 2a,c. The relative integral intensity (normalized to integral intensity with doping of 20% Yb, 1% Er) and green to red ratio at fixed 20% Yb^{3+} as a function of Er^{3+} concentration (ranging from 1 to 5%) are shown in Fig. 2b,d. The reported results from the existing experimental studies showed similar trends that the relative integral intensity rapidly decreases with increasing Yb^{3+} concentration (Fig. 2a) or Er^{3+} concentration (Fig. 2b). The difference in magnitude may be attributed to different excitation power and different synthesis processes of the nanoparticles. However, the simulation results from standard model show that the relative integral intensity increases with Yb^{3+} concentration before the concentration of Yb^{3+} reaches 20% and increases with Er^{3+} concentration in the considered range of Er^{3+} concentration (1–5%). Whereas, our modified model by incorporating self-quenching effect is capable of capturing the rapid downtrends in UC emission with increasing Yb^{3+} or Er^{3+} doping concentration as found in both experiments [4,5]. (Fig. 2a,b).

To provide the mechanistic insight into the concentration dependent change in UC emission intensity, we simplified Eq. (2) (Eqs. A1–A10 in Appendix A) to Eq. (C14) and demonstrated that EBT 3, EBT 4, and self-quenching effect of Yb^{3+} are the three major processes that are responsible for Yb^{3+} concentration quenching (Derivation processes See Appendix C). If there is no self-quenching effect (as in the case of standard model), the green emission intensity would not decrease so rapidly which contradicts with the existing experimental results as shown in Fig. 2a. We also simplified Eq. (2) (Eqs. A1–A10 in Appendix A) to Eq. C15 and demonstrated that self-quenching of Er^{3+} takes major responsibility for concentration quenching in Er^{3+} doping, which agrees with experimental results shown in Fig. 2b (Derivation processes See Appendix C). If there is no self-quenching effect (as in the case of standard model), the emission intensity will increase continuously with the increasing Er^{3+} concentration, which is not supported by experimental results (Fig. 2b). Only considering CR process could not explain Er^{3+} concentration quenching completely because ETU processes can also increase with doping

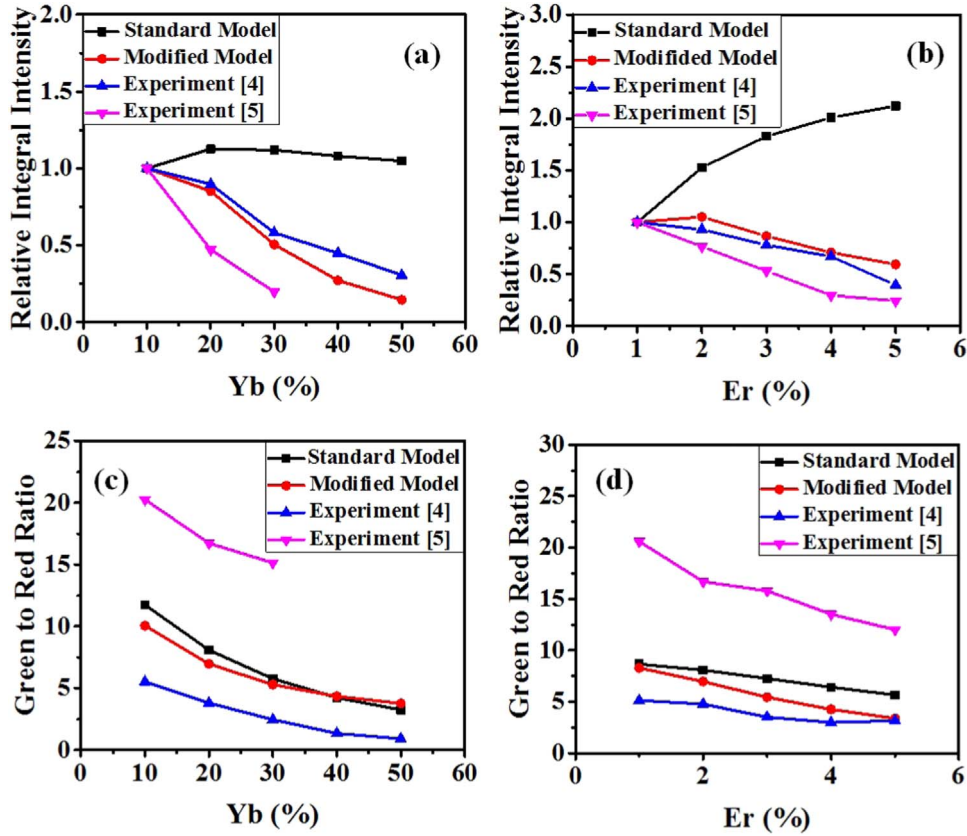


Fig. 2. Model verification. Dependence of integral UC emission (500–700 nm) intensity and green to red ratio as a function of Yb³⁺ concentration at fixed 2% Er³⁺ (a,c) and as a function of Er³⁺ concentration at fixed 20% Yb³⁺ (b,d). The simulation results are obtained at 980 nm (1 W · cm⁻²) excitation. (For interpretation of the references to color in this figure legend, the reader is referred to the web version of this article.)

concentration to offset the quenching effect of CR. Self-quenching process of Er³⁺ could accelerate the decreasing trend of UC emission intensity with increasing doping concentration.

To study the effect of CR process on relative UC intensity, we simulated the relative green emission intensity, red emission intensity and integral intensity, as a function of Er³⁺ concentration under different P_{CR} (CR rate constant) using standard model. The results indicate that relative green emission intensity would increase with increasing Er³⁺ concentration unless CR rate constant is larger than $P_{CR} \cdot 10$ (Fig. C1a, see Appendix C). This phenomenon may be attributed to reason that the rates of ETU2 and ETU4 both increase proportionally with Er³⁺ concentration which offsets the CR effect. While relative red emission intensity kept ascending with increasing concentration (Fig. C1b, see Appendix C). This may be attributed to that there are no CR process on red emission. When we compare the relative integral intensity of red and green emissions, the relative integral intensity shows ascending as Er³⁺ concentration increases (Fig. C1c, see Appendix C). These results suggest that if there is no selfquenching effect (as in the case of standard model), the UC emission intensity (especially for red) will increase continuously with the increasing Er³⁺ concentration.

To verify our hypothesis that the dependence of lifetime of ⁴S_{3/2} on Er³⁺ concentration quenching is mainly affected by self-quenching effect rather than CR of Er³⁺, we simulated the lifetime of ⁴S_{3/2} in single Er³⁺ doped β-NaYF₄. In the experiments by Suyver [9], the lifetime of ⁴S_{3/2} was measured under direct excitation (400 cm⁻¹ higher energy than the observed emission), thus we set the initial population of ⁴S_{3/2} as 0.1N_{Er0} and initial population of other excited states as zero to simulate this experimental condition. The calculated lifetime is shown in Table C1 (see Appendix C). We observed that CR process could partly explain

decreasing lifetime with increasing doping concentration. Without considering self-quenching, the lifetime decreases much slower than that in experiment. While self-quenching effect dominates the descending trend. This conclusion is also supported by the branch pathway analysis in modified model of ⁴S_{3/2} Table B1 (see Appendix B). We found that CR process branch ratio is 0.214 in β-NaYF₄:20%Yb, 2%Er, while self-quenching effect branch ratio is 0.617, which further suggests that self-quenching plays the main role in green states quenching when the Er³⁺ concentration is beyond 2%. We herein demonstrated that besides CR, self-quenching process is a main reason for concentration quenching effect.

3.3. Doping concentration dependence of green to red ratio

Experimental results show that green to red ratio decrease with increasing Yb³⁺ or Er³⁺ concentrations (Fig. 2c-d). Both the standard model and the modified model provide reasonable simulation results of green to red ratio. To understand the concentration dependent change in green to red ratio, we derived green to red ratio from Eq. (A6) (See Appendix A) as:

$$\begin{aligned} I_{\text{green}}/I_{\text{red}} &= A_{Er61}N_{Er6}/(A_{Er51}N_{Er5}) \\ &= A_{Er61}/A_{Er51} \left[W_{Er5}/W_{Er65}^{NR} - P_{ETU1}^{ET}N_{Er2}N_{Er3}/(W_{Er65}^{NR}N_{Er5}) \right. \\ &\quad \left. - P_{ETU3}N_{Er2}N_{Yb2}/(W_{Er65}^{NR}N_{Er5}) \right] \end{aligned} \quad (9)$$

Since decay constant W_{Er5} and W_{Er65}^{NR} will not change with varying doping concentrations, the decreasing of green to red ratio with increasing Er³⁺(Yb³⁺) concentration is mainly attributed to rate of ETU 1(ETU 3). (See Appendix D).

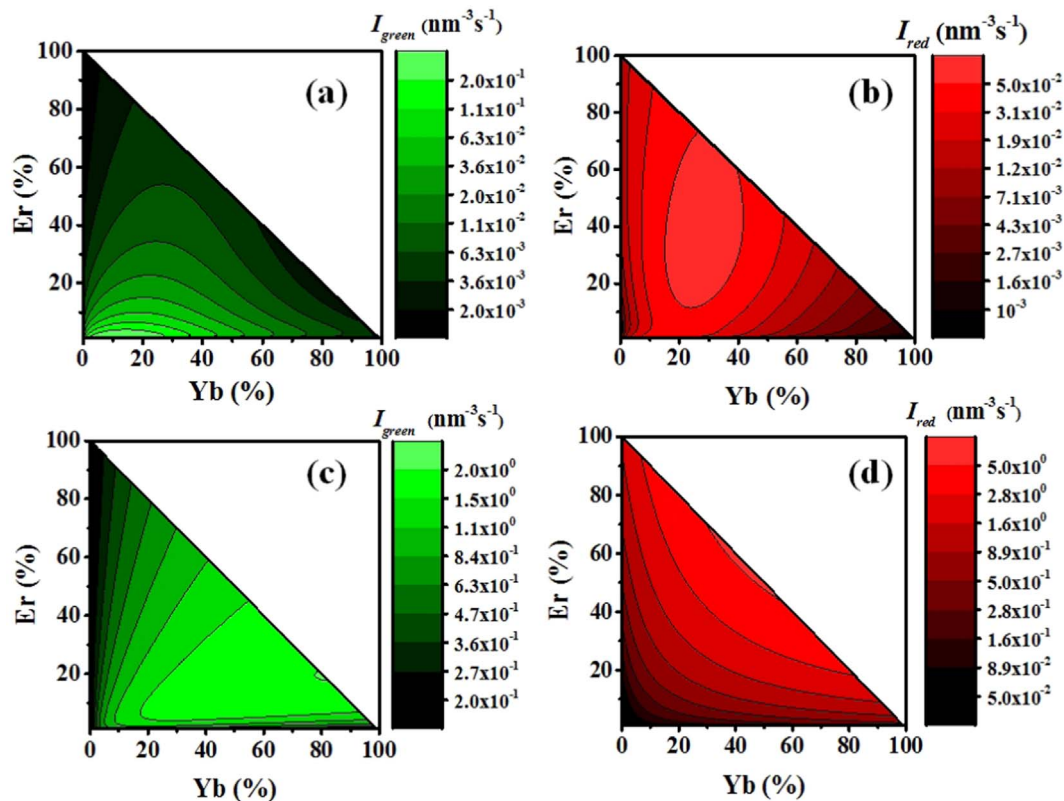


Fig. 3. Contour plots for green emission (a,c) and red emission (b,d) of β -NaYF₄ with Er³⁺ and Yb³⁺ concentrations varying from 1% to 100% under 980 nm (1 W · cm⁻²) excitation. (a,b) with consideration of self-quenching effect (modified model), (c,d) without consideration of self-quenching effect (standard model). (For interpretation of the references to color in this figure legend, the reader is referred to the web version of this article.)

3.4. Doping concentration contour plot of green and red emission intensity

A contour plot of emission intensity can be used to describe how green and red emissions vary with Yb³⁺ and Er³⁺ concentrations (Fig. 3). Green UC emission intensity I_{green} ($I_{green} = A_{Er6(1)}N_{Er6(1)} + A_{Er6(2)}N_{Er6(2)}$, where Er6⁽¹⁾ is ⁴S_{3/2} and Er6⁽²⁾ is ²H_{11/2}) and red UC emission intensity I_{red} ($I_{red} = A_{Er5}N_{Er5}$) are calculated along the doping triangle (Er³⁺: 1–100%, Yb³⁺: 0–99%) with doping concentration intervals of 1%. The optimal doping concentration for green emission was estimated to be 1% Er³⁺, 9% Yb³⁺ where I_{green} is equal to 0.455 nm⁻³ s⁻¹ (Fig. 3a). The optimal doping concentration for red emission was 34% Er³⁺, 27% Yb³⁺ (Fig. 3b) where I_{red} is equal to 0.0625 nm⁻³ s⁻¹. We also demonstrate that doping at 1% Er³⁺, 1% Yb³⁺ emits most pure green emission with green to red ratio of 18 (Fig. 3a), while doping at 100% Er³⁺, 0% Yb³⁺ emits most pure red emission with green to red ratio of 0.086 (Fig. 3b). For green emission, the simulation results show that lower Er³⁺ concentration contributes to higher green emission intensity (Fig. 3a). This phenomenon agrees well with experimental studies [4,5]. Whereas, in NaYbF₄:Er, higher Er³⁺ concentration is in favor of red emission (Fig. 3b) which also matches existing experimental results [8]. Herein, we demonstrate that our modified model provides a powerful tool for simulation of green and red emission as a function of doping concentration.

To explore to what extent upconversion emission can be affected by self-quenching effect, we set the self-quenching rate constant of Er³⁺ and Yb³⁺ to zero (this condition follows standard model exactly) and provided the green (Fig. 3c) and red emission (Fig. 3d) contour plots as a function of Yb³⁺ and Er³⁺ concentrations. We find that without consideration of self-quenching effect the optimal green and red emission intensities are nearly

4.4 times and 86 times higher than that with consideration of self-quenching effect corresponding to the optimal doping concentration at 81% Yb³⁺, 19% Er³⁺ (where I_{green} is equal to 2.01 nm⁻³ s⁻¹) and 43% Yb³⁺, 57% Er³⁺ (where I_{red} is equal to 5.37 nm⁻³ s⁻¹) respectively. Here we prove that self-quenching effect plays a major role in concentration quenching. Our results also confirm that the UC efficiency could be significantly improved by avoiding self-quenching (the migration of energy to defects). There have been some approaches proposed to engineer energy migration at sub-lattice level, such as synthesizing crystals with discrete zero-dimension doping clusters [25] and constructing thin intra shells to suppress energy migration [26], which pave ways to overcome self-quenching effect. It could be expected that in an ideal matrix where self-quenching has been efficient limited, the UC emission would no longer be limited by doping concentration.

3.5. Excitation power dependence of UC emission

To understand the excitation power dependent change in integral emission intensity and the corresponding change in green to red ratio, we explored the dependence of integral emission intensity (Fig. 4a) and green to red ratio (Fig. 4b) on Er³⁺ concentration at a fixed Yb³⁺ concentration (20%). Since higher excitation power may lead to non-ignorable influence of higher energy levels of Er³⁺ [22], we limited our model to low excitation power (< 10² W · cm⁻²). Our simulation results show that at low excitation power, the optimal Er³⁺ concentration remains almost unchanged with varying excitation power (Fig. 4a), which agrees well with the reported results [22]. This indicates that the optimal concentration for integral emission could be considered as a constant of excitation power at low excitation condition. Our simulation results also show that green to red ratio decreases with

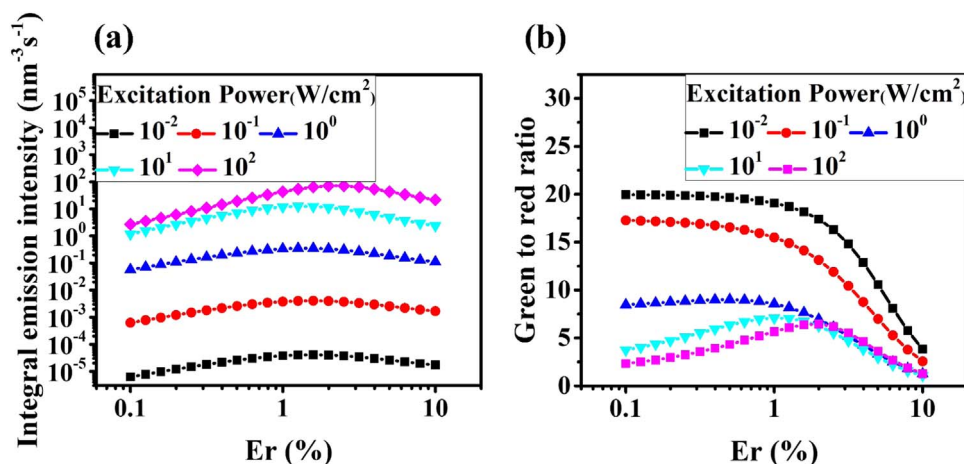


Fig. 4. Dependence of integral emission intensity (500 nm to 700 nm) (a) and green to red ratio (b) on the Er³⁺ concentration at excitation power ranging from 10⁻² to 10² W·cm⁻². (For interpretation of the references to color in this figure legend, the reader is referred to the web version of this article.)

increasing excitation power (Fig. 4b), thus the difference in green to red ratio between the two experimental results (Fig. 2b,d) could be attributed to different excitation conditions.

4. Conclusions

We developed a modified energy transfer model by considering the self-quenching effect for simulation of UC emission and applied this model to explain the rapid concentration quenching phenomena of Yb³⁺ and Er³⁺ co-doped UC phosphors. Our results demonstrate that self-quenching effect plays a critical role in concentration quenching and UC emission efficiency could be improved by avoiding self-quenching effect. Our model provides a powerful tool for simulating UC emission of various lanthanide doped UC phosphors and pave the way for designing matrix for high efficient UC emission.

Acknowledgements

This work was financially supported by the National Natural Science Foundation of China (11402192) and Fundamental Research Funds for the Central Universities (2016qngz03).

Appendix A. Supplementary material

Supplementary data associated with this article can be found in the online version at <http://dx.doi.org/10.1016/j.jlumin.2017.01.025>.

References

- [1] B. Zhou, B. Shi, D. Jin, X. Liu, Nat. Nano 10 (2015) 924–936.
- [2] F. Wang, X. Liu, Chem. Soc. Rev. 38 (2009) 976–989.
- [3] E.M. Chan, E.S. Levy, B.E. Cohen, Adv. Mater. 27 (2015) 5753–5761.
- [4] L. Liang, H. Wu, H. Hu, M. Wu, Q. Su, J. Alloy. Compd. 368 (2004) 94–100.
- [5] H.-X. Mai, Y.-W. Zhang, L.-D. Sun, C.-H. Yan, J. Phys. Chem. C 111 (2007) 13721–13729.
- [6] V. Mahalingam, C. Hazra, R. Naccache, F. Vetrone, J.A. Capobianco, J. Mater. Chem. C 1 (2013) 6536–6540.
- [7] G. Chen, G. Somesfalean, Y. Liu, Z. Zhang, Q. Sun, F. Wang, Phys. Rev. B 75 (2007) 195204.
- [8] W. Wei, Y. Zhang, R. Chen, J. Goggi, N. Ren, L. Huang, K.K. Bhakoo, H. Sun, T.T. Y. Tan, Chem. Mater. 26 (2014) 5183–5186.
- [9] J.F. Suyver, J. Grimm, M.K. van Veen, D. Biner, K.W. Krämer, H.U. Güdel, J. Lumin. 117 (2006) 1–12.
- [10] T. Li, C. Guo, L. Li, Opt. Express 21 (2013) 18281–18289.
- [11] F. Auzel, F. Bonfigli, S. Gagliari, G. Baldacchini, J. Lumin 94–95 (2001) 293–297.
- [12] F. Auzel, G. Baldacchini, L. Laversenne, G. Boulon, Opt. Mater. 24 (2003) 103–109.
- [13] F. Auzel, Chem. Rev. 104 (2003) 139–174.
- [14] F. Auzel, F. Pellé, J. Lumin. 69 (1996) 249–255.
- [15] P. Villanueva-Delgado, K.W. Krämer, R. Valiente, J. Phys. Chem. C 119 (2015) 23648–23657.
- [16] X. Huang, D. Chen, L. Lin, Z. Wang, Y. Wang, Z. Feng, Z. Zheng, Sci. China Phys. Mech. 55 (2012) 1148–1151.
- [17] S. Fischer, H. Steinkemper, P. Löper, M. Hermlé, J.C. Goldschmidt, J. Appl. Phys. 111 (2012) 013109.
- [18] E.M. Chan, D.J. Gargas, P.J. Schuck, D.J. Milliron, J. Phys. Chem. B 116 (2012) 10561–10570.
- [19] D. Lu, S.K. Cho, S. Ahn, L. Brun, C.J. Summers, W. Park, ACS Nano (2014).
- [20] R.B. Anderson, S.J. Smith, P.S. May, M.T. Berry, J. Phys. Chem. Lett. 5 (2013) 36–42.
- [21] M.T. Berry, P.S. May, J. Phys. Chem. A 119 (2015) 9805–9811.
- [22] D.J. Gargas, E.M. Chan, A.D. Ostrowski, S. Aloni, M.V.P. Altoe, E.S. Barnard, B. Sanii, J.J. Urban, D.J. Milliron, B.E. Cohen, P.J. Schuck, Nat. Nano 9 (2014) 300–305.
- [23] T. Jung, H.L. Jo, S.H. Nam, B. Yoo, Y. Cho, J. Kim, H.M. Kim, T. Hyeon, Y.D. Suh, H. Lee, Phys. Chem. Chem., Phys. 17 (2015) 13201–13205.
- [24] F. Wang, F. Song, G. Zhang, Y. Han, Q. Li, C. Ming, J. Tian, J. Appl. Phys. 115 (2014) 134310.
- [25] J. Wang, R. Deng, M.A. MacDonald, B. Chen, J. Yuan, F. Wang, D. Chi, T.S. Andy Hor, P. Zhang, G. Liu, Y. Han, X. Liu, Nat. Mater. 13 (2014) 157–162.
- [26] X. Chen, L. Jin, W. Kong, T. Sun, W. Zhang, X. Liu, J. Fan, S.F. Yu, F. Wang, Nat. Commun. 7 (2016).